Nonlinear light propagation in chalcogenide photonic crystal slow light waveguides

Keijiro Suzuki,[1,2] and Toshihiko Baba[1,2,*]

[1]*Department of Electrical and Computer Engineering, Yokohama National University, 79-5 Tokiwadai, Hodogaya-ku, Yokohama, 240-8501, Japan*
[2]*Core Research for Evolutional Science and Technology, Japan Science and Technology Agency, 5 Sanbancho, Chiyoda-ku, Tokyo, 102-0075, Japan*
**baba@ynu.ac.jp*

Abstract: Optical nonlinearity can be enhanced by the combination of highly nonlinear chalcogenide glass and photonic crystal waveguides (PCWs) providing strong optical confinement and slow-light effects. In a Ag-As_2Se_3 chalcogenide PCW, the effective nonlinear parameter γ_{eff} reaches 6.3×10^4 $W^{-1}m^{-1}$, which is 200 times larger than that in Si photonic wire waveguides. In this paper, we report the detailed design, fabrication process, and the linear and nonlinear characteristics of this waveguide at silica fiber communication wavelengths. We show that the waveguide exhibits negligible two-photon absorption, and also high-efficiency self-phase modulation and four-wave mixing, which are assisted by low-dispersion slow light.

OCIS codes: (230.5298) Photonic crystals; (230.4320) Nonlinear optical devices; (160.2750) Glass and other amorphous materials; (230.3120) Integrated optics devices.

References and links

1. R. Salem, M. A. Foster, A. C. Turner, D. F. Geraghty, M. Lipson, and A. L. Gaeta, "Signal regeneration using low-power four-wave mixing on silicon chip," Nat. Photonics **2**(1), 35–38 (2008).
2. R. E. Slusher, G. Lenz, J. Hodelin, J. Sanghera, L. B. Shaw, and I. D. Aggarwal, "Large Raman gain and nonlinear phase shifts in high-purity As_2Se_3 chalcogenide fibers," J. Opt. Soc. Am. B **21**(6), 1146–1155 (2004).
3. M. D. Pelusi, F. Luan, E. Magi, M. R. Lamont, D. J. Moss, B. J. Eggleton, J. S. Sanghera, L. B. Shaw, and I. D. Aggarwal, "High bit rate all-optical signal processing in a fiber photonic wire," Opt. Express **16**(15), 11506–11512 (2008).
4. F. Luan, M. D. Pelusi, M. R. E. Lamont, D.-Y. Choi, S. Madden, B. Luther-Davies, and B. J. Eggleton, "Dispersion engineered As_2S_3 planar waveguides for broadband four-wave mixing based wavelength conversion of 40 Gb/s signals," Opt. Express **17**(5), 3514–3520 (2009).
5. H. Yamada, M. Shirane, T. Chu, H. Yokoyama, S. Ishida, and Y. Arakawa, "Nonlinear-optic silicon-nanowire waveguides," Jpn. J. Appl. Phys. **44**(9A), 6541–6545 (2005).
6. E. Dulkeith, Y. A. Vlasov, X. Chen, N. C. Panoiu, and R. M. Osgood, Jr., "Self-phase-modulation in submicron silicon-on-insulator photonic wires," Opt. Express **14**(12), 5524–5534 (2006).
7. K. Narayanan, and S. F. Preble, "Optical nonlinearities in hydrogenated-amorphous silicon waveguides," Opt. Express **18**(9), 8998–9005 (2010).
8. I. W. Hsieh, X. G. Chen, J. I. Dadap, N. C. Panoiu, R. M. Osgood, S. J. McNab, and Y. A. Vlasov, "Ultrafast-pulse self-phase modulation and third-order dispersion in Si photonic wire-waveguides," Opt. Express **14**(25), 12380–12387 (2006).
9. H. Rong, Y.-H. Kuo, A. Liu, M. Paniccia, and O. Cohen, "High efficiency wavelength conversion of 10 Gb/s data in silicon waveguides," Opt. Express **14**(3), 1182–1188 (2006).
10. H. Fukuda, K. Yamada, T. Shoji, M. Takahashi, T. Tsuchizawa, T. Watanabe, J. Takahashi, and S. Itabashi, "Four-wave mixing in silicon wire waveguides," Opt. Express **13**(12), 4629–4637 (2005).
11. G. A. Siviloglou, S. Suntsov, R. El-Ganainy, R. Iwanow, G. I. Stegeman, D. N. Christodoulides, R. Morandotti, D. Modotto, A. Locatelli, C. De Angelis, F. Pozzi, C. R. Stanley, and M. Sorel, "Enhanced third-order nonlinear effects in optical AlGaAs nanowires," Opt. Express **14**(20), 9377–9384 (2006).
12. K. Inoue, H. Oda, N. Ikeda, and K. Asakawa, "Enhanced third-order nonlinear effects in slow-light photonic-crystal slab waveguides of line-defect," Opt. Express **17**(9), 7206–7216 (2009).
13. R. G. DeCorby, N. Ponnampalam, M. M. Pai, H. T. Nguyen, P. K. Dwivedi, T. J. Clement, C. J. Haugen, J. N. McMullin, and S. O. Kasap, "High index contrast waveguides in chalcogenide glass and polymer," IEEE J. Sel. Top. Quantum Electron. **11**(2), 539–546 (2005).

#134309 - $15.00 USD Received 31 Aug 2010; revised 22 Sep 2010; accepted 23 Sep 2010; published 6 Dec 2010

14. V. K. Tikhomirov, D. Furniss, A. B. Seddon, J. A. Savage, P. D. Mason, D. A. Orchard, and K. L. Lewis, "Glass formation in the Te-enriched part of the quaternary Ge-As-Se-Te system and its implication for mid-infrared optical fibres," Infrared Phys. Technol. **45**(2), 115–123 (2004).
15. J. M. Harbold, F. Ö. Ilday, F. W. Wise, J. S. Sanghera, V. Q. Nguyen, L. B. Shaw, and I. D. Aggarwal, "Highly nonlinear As-S-Se glasses for all-optical switching," Opt. Lett. **27**(2), 119–121 (2002).
16. M. Dinu, F. Quochi, and H. Garcia, "Third-order nonlinearities in silicon at telecom wavelengths," Appl. Phys. Lett. **82**(18), 2954–2956 (2003).
17. A. Zakery, and S. R. Elliott, *Optical Nonlinearities in Chalcogenide Glasses and their Applications* (Springer, New York, 2007).
18. D. A. P. Bulla, R. P. Wang, A. Prasad, A. V. Rode, S. J. Madden, and B. Luther-Davies, "On the properties and stability of thermally evaporated Ge-As-Se thin films," Appl. Phys., A Mater. Sci. Process. **96**(3), 615–625 (2009).
19. S. Song, J. Dua, and C. B. Arnold, "Influence of annealing conditions on the optical and structural properties of spin-coated As_2S_3 chalcogenide glass thin films," Opt. Express **18**(6), 5472–5480 (2010).
20. T. G. Robinson, R. G. DeCorby, J. N. McMullin, C. J. Haugen, S. O. Kasap, and D. Tonchev, "Strong Bragg gratings photoinduced by 633-nm illumination in evaporated As_2Se_3 thin films," Opt. Lett. **28**(6), 459–461 (2003).
21. A. V. Rode, A. Zakery, M. Samoc, R. B. Charters, E. G. Gamaly, and B. Luther-Davies, "Laser-deposited As_2S_3 chalcogenide films for waveguide applications," Appl. Surf. Sci. **197**, 481–485 (2002).
22. D. Freeman, C. Grillet, M. W. Lee, C. L. C. Smith, Y. Ruan, A. Rode, M. Krolikowska, S. Tomljenovic-Hanic, C. M. De Sterke, M. J. Steel, B. Luther-Davies, S. Madden, D. J. Moss, Y. H. Lee, and B. J. Eggleton, "Chalcogenide glass photonic crystals," Photon. Nanostructures **6**(1), 3–11 (2008).
23. T. Baba, "Slow light in photonic crystals," Nat. Photonics **2**(8), 465–473 (2008).
24. B. Corcoran, C. Monat, C. Grillet, D. J. Moss, B. J. Eggleton, T. P. White, L. O'Faolain, and T. F. Krauss, "Green light emission in silicon through slow-light enhanced third-harmonic generation in photonic-crystal waveguides," Nat. Photonics **3**(4), 206–210 (2009).
25. Y. Hamachi, S. Kubo, and T. Baba, "Slow light with low dispersion and nonlinear enhancement in a lattice-shifted photonic crystal waveguide," Opt. Lett. **34**(7), 1072–1074 (2009).
26. C. Monat, B. Corcoran, D. Pudo, M. Ebnali-Heidari, C. Grillet, M. D. Pelusi, D. J. Moss, B. J. Eggleton, T. P. White, L. O'Faolain, and T. F. Krauss, "Slow light enhanced nonlinear optics in silicon photonic crystal waveguides," IEEE J. Sel. Top. Quantum Electron. **16**(1), 344–356 (2010).
27. J. F. McMillan, M. Yu, D.-L. Kwong, and C. W. Wong, "Observation of four-wave mixing in slow-light silicon photonic crystal waveguides," Opt. Express **18**(15), 15484–15497 (2010).
28. V. Eckhouse, I. Cestier, G. Eisenstein, S. Combrié, P. Colman, A. De Rossi, M. Santagiustina, C. G. Someda, and G. Vadalà, "Highly efficient four wave mixing in GaInP photonic crystal waveguides," Opt. Lett. **35**(9), 1440–1442 (2010).
29. A. Baron, A. Ryasnyanskiy, N. Dubreuil, P. Delaye, Q. Vy Tran, S. Combrié, A. de Rossi, R. Frey, and G. Roosen, "Light localization induced enhancement of third order nonlinearities in a GaAs photonic crystal waveguide," Opt. Express **17**(2), 552–557 (2009).
30. I. Cestier, V. Eckhouse, G. Eisenstein, S. Combrié, P. Colman, and A. De Rossi, "Resonance enhanced large third order nonlinear optical response in slow light GaInP photonic-crystal waveguides," Opt. Express **18**(6), 5746–5753 (2010).
31. D. Freeman, S. Madden, and B. Luther-Davies, "Fabrication of planar photonic crystals in a chalcogenide glass using a focused ion beam," Opt. Express **13**(8), 3079–3086 (2005).
32. Y. Ruan, M.-K. Kim, Y.-H. Lee, B. Luther-Davies, and A. Rode, "Fabrication of high-Q chalcogenide photonic crystal resonators by *e*-beam lithography," Appl. Phys. Lett. **90**(7), 071102 (2007).
33. A. Feigel, M. Veinger, B. Sfez, A. Arsh, M. Klebanov, and V. Lyubin, "Two dimensional photonic band gap pattering in thin chalcogenide glassy films," Thin Solid Films **488**(1–2), 185–188 (2005).
34. A. Popescu, S. Miclos, D. Savastru, R. Savastru, M. Ciobanu, M. Popescu, A. Lorinczi, F. Sava, A. Velea, F. Jipa, and M. Zamfirescu, "Direct laser writing of two-dimensional photonic structures in amorphous As_2S_3 thin films," J. Optoelectron. Adv. Mater. **11**(11), 1874–1880 (2009).
35. K. Paivasaari, V. K. Tikhomirov, and J. Turunen, "High refractive index chalcogenide glass for photonic crystal applications," Opt. Express **15**(5), 2336–2340 (2007).
36. K. Suzuki, Y. Hamachi, and T. Baba, "Fabrication and characterization of chalcogenide glass photonic crystal waveguides," Opt. Express **17**(25), 22393–22400 (2009).
37. K. Ogusu, J. Yamasaki, S. Maeda, M. Kitao, and M. Minakata, "Linear and nonlinear optical properties of Ag-As-Se chalcogenide glasses for all-optical switching," Opt. Lett. **29**(3), 265–267 (2004).
38. L. O'Faolain, T. P. White, D. O'Brien, X. Yuan, M. D. Settle, and T. F. Krauss, "Dependence of extrinsic loss on group velocity in photonic crystal waveguides," Opt. Express **15**(20), 13129–13138 (2007).
39. T. Wágner, V. Perina, A. Mackova, E. Rauhala, A. Seppala, M. Vleck, S. O. Kasap, M. Vlcek, and M. Frumar, "The tailoring of the composition of Ag-As-S amorphous films using photo-induced solid state reaction between Ag and $As_{30}S_{70}$ films," Solid State Ion. **141**(1), 387–395 (2001).
40. K. Ogusu, S. Maeda, M. Kitao, H. Li, and M. Minakata, "Optical and structural properties of Ag(Cu)-As_2Se_3 chalcogenide films prepared by a photodoping," J. Non-Cryst. Solids **347**(1–3), 159–165 (2004).
41. J. Adachi, N. Ishikura, H. Sasaki, and T. Baba, "Wide range tuning of slow light pulse in SOI photonic crystal coupled waveguide via folded chirping," IEEE J. Sel. Top. Quantum Electron. **16**(1), 192–199 (2010).

#134309 - $15.00 USD Received 31 Aug 2010; revised 22 Sep 2010; accepted 23 Sep 2010; published 6 Dec 2010

42. C. Monat, B. Corcoran, M. Ebnali-Heidari, C. Grillet, B. J. Eggleton, T. P. White, L. O'Faolain, and T. F. Krauss, "Slow light enhancement of nonlinear effects in silicon engineered photonic crystal waveguides," Opt. Express **17**(4), 2944–2953 (2009).
43. T. Vallaitis, S. Bogatscher, L. Alloatti, P. Dumon, R. Baets, M. L. Scimeca, I. Biaggio, F. Diederich, C. Koos, W. Freude, and J. Leuthold, "Optical properties of highly nonlinear silicon-organic hybrid (SOH) waveguide geometries," Opt. Express **17**(20), 17357–17368 (2009).

1. Introduction

In recent years, optical network traffic and its electrical power consumption have increased very rapidly. To deal with future growth, more advanced transmission systems, particularly photonic routers, are anticipated. Wavelength routing has been studied as one of the candidate solutions, but it requires highly efficient wavelength convertors. Although cross-phase modulation and four-wave mixing (FWM) are promising techniques [1], they generally require high operating power and/or long device length due to limited material nonlinearities. Figure 1 summarizes the operating power and the lengths of various nonlinear devices. Fiber-based devices are easy to fabricate and evaluate. However, low power density in their large core is disadvantageous for nonlinearities, and so it must be compensated by a device length longer than centimeters [2,3]. On-chip optical waveguides, on the other hand, are advantageous for enhancing the power density, shortening the device, and integration with other components. FWM induced by third-order nonlinearity has been observed in a 6-cm-long As_2S_3 chalcogenide glass rib waveguide at an input power of less than 1 W [4]. Various nonlinearities have also been demonstrated for Si photonic wire waveguides. This type of waveguide can particularly enhance the power density, due to its strong optical confinement into the high index contrast tiny core [5–8]. In Si-based waveguides, however, the nonlinearity mainly arises from carrier effects generated by two-photon absorption (TPA), which results in a high loss and a response time limited by the carrier lifetime. Although FWM was observed at several hundreds of mW where the TPA was negligible, a long waveguide of 5 cm was necessary [9,10]. In 600-μm-long AlGaAs wire waveguides whose aluminum content was increased to suppress the TPA at silica-fiber communication wavelengths, e.g. λ ~1.55 μm, the self-phase modulation (SPM) was observed at a 30 W input power [11]. The same material was also processed into photonic crystal waveguides (PCWs), and the power required for the same SPM was reduced to 3.5 W by exploiting slow-light effects [12]. Thus, we can expect slow-light PCWs made of highly nonlinear materials without TPA to be a suitable platform of nonlinear devices satisfying low-power operation, short length and carrier-free high-speed response.

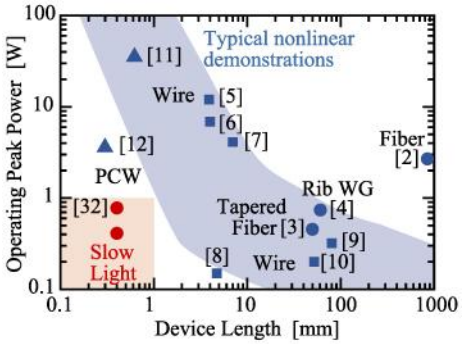

Fig. 1. Relation of operating power and device length for optical nonlinearity such as SPM (1.5 π nonlinear phase shift) and FWM in various material waveguides. Circles, square, and triangle denote ChG, Si, and III-V materials, respectively.

When chalcogenide glasses (ChGs) are used as base materials for nonlinear devices at λ ~1.55 μm, S- and Se-based glasses mixed with As and/or Ge are often employed. They have the following attractive properties:

#134309 - $15.00 USD Received 31 Aug 2010; revised 22 Sep 2010; accepted 23 Sep 2010; published 6 Dec 2010

i) These ChGs have a broad transparent window from λ = 0.8 – 20 μm [13,14] and ultrahigh-speed third-order nonlinear response (< 100 fs) without carrier effects.

ii) They exhibit a large third-order nonlinear index n_2 simultaneously with low TPA coefficient β at λ ~1.55 μm. The nonlinear figure of merit FOM (≡ $n_2/\beta\lambda$) is 11 for bulk As_2Se_3 [15], while 0.4 for bulk Si [16].

iii) Their films can be fabricated at low temperature (< 400°C) [17–19], which is compatible to back-end process in Si-photonics.

iv) Illuminated by light around the absorption edge, some photo-induced phenomena occur. One of these, photodarkening, can be used for the fabrication and post-tuning of devices [20–22].

PCWs are formed by introducing a single line-defect into air-bridge photonic crystal slab, which consists of two-dimensionally periodic array of airholes in a triangular lattice. Their small modal cross-section and low group velocity v_g of light, namely *slow light*, can enhance the optical intensity in the waveguides [23]. In particular, low dispersion slow light (we call it *LD slow light*) is obtained in optimized structures, and the nonlinearity is enhanced through the spatial compression of short optical pulses. In fact, the enhancement of SPM, TPA, FWM and third harmonic generation has been observed in Si slow-light PCWs [24–27] and GaAs, AlGaAs and GaInP ones [12, 28–30].

Challenges to fabricating ChG photonic crystals have been reported with various ChGs and fabrication process, such as the combination of $Ge_{33}As_{12}Se_{55}$ with focused ion beam milling [31], that with *e*-beam lithography and chemically assisted ion beam etching [32], As_2S_3 with holographic lithography and wet etching [33], and As_2S_3 and $Ge_{20}As_{20}Se_{14}Te_{46}$ with direct laser writing [34,35]. In general, however, it is not straightforward to form waveguide facets and vertical airholes of photonic crystals because of the softness of ChGs, which makes optical characterizations challenging. Previously, we fabricated Ag-As_2Se_3 PCWs using *e*-beam lithography and inductively coupled plasma (ICP) etching, and reported their linear and nonlinear characteristics, for the first time, although they were limited in the high v_g regime [36]. This material is known to have n_2 of 9.0×10^{-17} m^2/W at λ = 1.05 μm [37], which is the highest value ever reported for ChGs. Therefore, Ag-As_2Se_3 and LD slow-light PCW can be one of the most powerful combination toward the present purpose.

In this paper, we comprehensively discuss the Ag-As_2Se_3 PCW in both high and low v_g regimes. We first show the design of lattice-shifted PCWs (LS-PCWs) suitable for LD slow-light generation [25]. We have developed this type of waveguide for Si. In this study, we optimized it for the ChG through the photonic band analysis. Next, we describe the fabrication process in detail, which enables us to observe the clear propagation characteristics against continuous light and short pulses in the linear regime. Finally, we present the nonlinear characteristics such as TPA, SPM and FWM against short pulse pumping, discuss their dependency on slow light and compare with those in Si waveguides.

2. Design

In the LS-PCW, the third rows of airholes from the line defect are shifted parallel to the line defect. The photonic band diagram of the Ag-As_2Se_3 ChG LS-PCW is calculated by using three-dimensional finite-deference time-domain method with periodic boundaries. We assume the material index of Ag-As_2Se_3 to be 2.85, which was deduced from the fitting of calculated band-edge wavelengths with experimental ones. We set the slab thickness as 300 nm to satisfy the single mode condition in the vertical direction and to obtain sufficient mechanical strength. Compared with Si (n ~3.5) PCWs, the small material index shifts the guided mode band to higher frequencies. Considering our measurement facilities shown later, we targeted the light propagation at λ ~1.55 μm, and chose a large lattice constant of a = 480 nm and a small normalized airhole diameter of $2r/a$ = 0.55.

#134309 - $15.00 USD Received 31 Aug 2010; revised 22 Sep 2010; accepted 23 Sep 2010; published 6 Dec 2010

Figure 2 shows the calculated results for different normalized shifts s/a. At $s/a = 0$, a round shape photonic band sandwiched by air light line and band-edge is observed. Increasing s/a, this band is raised by slab mode bands at lower frequencies, and the LD slow-light band characterized by a gentle slope (low v_g) and nearly straight part (low dispersion) appears. When s/a is relatively small, the group index n_g ($\equiv c/v_g = c(dk/d\omega)$, c: light speed in vacuum) giving the slowdown factor and the bandwidth $\Delta\lambda$ of LD slow-light are large and narrow, respectively. As s/a increases, n_g decreases and $\Delta\lambda$ broadens due to the essential constraint of slow light, and the flat band appears on the high frequency side. As s/a increases further, the flat band is almost fixed and the band-edge shifts to high frequency side. Consequently, n_g increases and $\Delta\lambda$ narrows again. In each LD slow-light band, n_g takes its minimum around the center wavelength. Table 1 summarizes the minimum n_g, $\Delta\lambda$ giving 0 – 10% change in n_g, and the normalized delay-bandwidth product $n_g\Delta\lambda/\lambda$ giving the slow-light performance [23]. The $n_g\Delta\lambda/\lambda$ varies from 0.33 – 0.14, which is almost similar to Si-PCWs' [25]. Larger n_g enhances the nonlinearity more, but narrower $\Delta\lambda$ restricts the observation of SPM and FWM. In addition, the extrinsic loss caused by structural disordering becomes severe at $n_g > 30$ [38]. Therefore, we targeted n_g and $\Delta\lambda$ at $s/a = 0.48$ in Table 1.

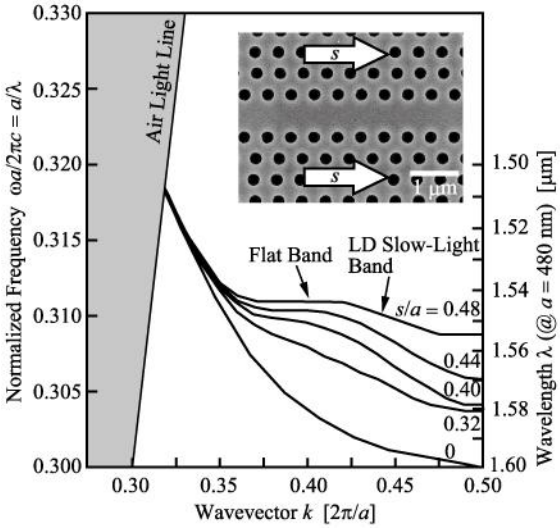

Fig. 2. Photonic band diagram of Ag-As_2Se_3 LS-PCW. Inset shows scanning electron micrograph (SEM) of fabricated ChG LS-PCW.

Table 1. Calculated group index, bandwidth and normalized delay-bandwidth product of Ag-As_2Se_3 LS-PCW.

s/a	n_g	$\Delta\lambda$ [nm]	$n_g\Delta\lambda/\lambda$
0.32	19	27	0.33
0.40	14	23	0.20
0.44	15	17	0.16
0.48	28	8	0.14

3. Fabrication

In the fabrication of Ag-As_2Se_3 PCW, we employ InP substrate for easy formation of waveguide facets by cleavage. First, 10-nm-thick Ti is thermally evaporated on the substrate at a deposition rate of 0.01 nm/s. This film is used for improving the adhesion of Ag-As_2Se_3 and InP. Since the melting point and vapor pressure are different between Ag and As_2Se_3, we cannot directly deposit Ag-As_2Se_3 using thermal evaporation of ternary source. Therefore, we evaporate 300-nm-thick As_2Se_3 at 0.2 nm/s, followed by 10-nm-thick Ag at 0.01 nm/s. To form Ag-As_2Se_3, they are interfused by photodoping technique [39], i.e. illuminating light

#134309 - $15.00 USD Received 31 Aug 2010; revised 22 Sep 2010; accepted 23 Sep 2010; published 6 Dec 2010

from halogen lamp for 30 min. Unlike thermal diffusion, Ag distributes almost uniformly in depth [40], and on this condition, Ag concentration becomes 5 at.%.

The PCW pattern is formed by using *e*-beam lithography with ~500-nm-thick positive resist (ZEON ZEP-520A) charge-dissipating agent (Showa-Denko Espacer-300Z) and 50 kV *e*-beam writer (Elionix ELS7500-EX). The pattern is transferred to the Ag-As_2Se_3 layer using ICP etching with CF_4: CHF_3 = 4: 1 gas mixture. The main etching gas is CF_4, while CHF_3 is used to deposit a thin polymer layer for protecting airhole sidewalls against neutral radicals in the plasma. It should be noted, however, that the excess deposition degrades the uniformity of airholes. To find a good balance, we optimized flow rates of these gases. The detail of the results is shown in the next section. To remove the resist after the etching, the substrate is boiled in a resist remover (ZEON ZDMAC) and cleaned in ultra-sonic bath. Finally, waveguide facets are formed by cleavage, and the air-bridge slab is formed by HF etching of Ti at room temperature and HCl: H_2O = 4: 1 etching of InP at 4 °C.

4. Linear characteristics

In all the measurements in this the following two sections, laser light is transverse-electric polarized, and coupled to the cleaved facet of 400-μm-long samples using microscope objectives. Output light is directly coupled to lensed fiber or fiber-coupled via another objective lenses. Light sources and other equipments are different between measurements.

A. Transmission spectra and etching condition

For the transmission spectrum in the linear regime, CW light from tunable laser is incident on the device. Output light is measured using optical power meter.

Let us discuss the dependence of the airhole cross-section and transmission spectrum on the gas flow rate in the ICP etching. Figure 3 shows the results of normal PCWs (s = 0). It is seen from the comparison between (a) and (b) that CHF_3 effectively suppresses the side etching, flattens the sidewalls, and improves the uniformity of airhole diameter 2r. This greatly suppresses unwanted oscillation in the transmission spectrum, makes spectral drops at the air light line and band-edge clearer, and improves the transmissivity by more than 5 dB. When the fraction of CHF_3 is increased while maintaining the total gas flow, excess deposition of the polymer degrades the sidewall angle and uniformity. (c) shows the results for the same gas fractions and higher total flow rate. Since the high flow rate suppresses the excess deposition, it makes the sidewall almost vertical, sharpens the spectral drop at the band-edge, and further improves the transmissivity. On this condition, the rms error in 2r is 4.4 nm, which is larger than 1.7 nm we evaluated for Si PCWs previously. Although we cannot increase gas flow rates any more in the current ICP machine, we expect a higher flow rate to provide better uniformity.

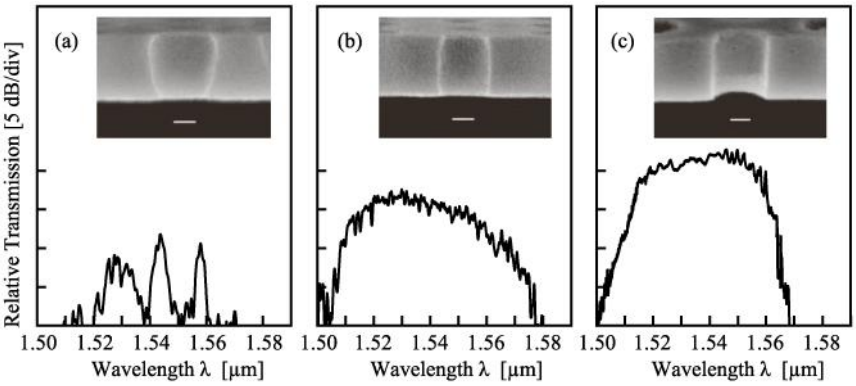

Fig. 3. Transmission spectrum of fabricated ChG PCW and SEM image of airhole cross-section for different gas flow rates in the ICP etching. White bar in the SEM images show a length of 100 nm. (a) CF_4: CHF_3 = 5: 0 sccm. (b) 4: 1 sccm. (c) 40: 10 sccm.

#134309 - $15.00 USD Received 31 Aug 2010; revised 22 Sep 2010; accepted 23 Sep 2010; published 6 Dec 2010

B. Transmission and group index spectra

Figure 4 shows the transmission and n_g spectra of LS-PCWs with different s and $2r$. For the latter, n_g is estimated using modulation phase-shift method [41], where tunable laser light is modulated sinusoidally and the signal phase of output light is measured to estimate the group delay and n_g.

(a) is the case without lattice shift (s = 0). It exhibits a typical spectrum of the PCW, in which n_g increases near the band-edge. Ideally, the increase is very rapid and the final n_g diverges to infinity. However, the maximum n_g measured is 42, and the spectral width from 20 – 80% of the maximum is 1.5 nm, which is wider than 0.5 nm in Si-PCWs [25]. It reflects the disordering in airhole diameters $2r$.

(b) - (d) are the cases with the lattice shift. They exhibit the LD slow light on the long wavelength side of the high v_g regime. A dip between them corresponds to the flat band in Fig. 2. Since a huge n_g and drastic modal change occur at the flat band, the transmission loss is large and n_g cannot be measured. The oscillation in the n_g spectra is primarily caused by the Fabry-Perot resonance between waveguide facets. In the LD slow-light band shown by light red color, n_g and $\Delta\lambda$ change similarly to those listed in Table 1; n_g ~15 with $\Delta\lambda$ ~25 nm ($n_g\Delta\lambda/\lambda$ ~0.24) at s/a = 0.33, n_g ~20 with $\Delta\lambda$ ~15 nm ($n_g\Delta\lambda/\lambda$ ~0.19) at s/a = 0.43 and n_g ~35 with $\Delta\lambda$ ~4 nm ($n_g\Delta\lambda/\lambda$ ~0.09) at s/a = 0.47.

The loss of the 400-μm-long device at the high v_g regime was estimated to be 5.4 dB, suggesting 5.4 dB / 0.400 mm = 14 dB/mm propagation loss α [36]. In the LD slow-light regime, relative transmission of each sample decreases to 3, 3 and 7 dB lower than that for high v_g regime, respectively. From these results, we can deduce α at the LD slow-light band: α = 8.4 dB / 0.400 mm = 21 dB/mm at n_g ~15 and 20; and α = 12.4 dB / 0.400 mm = 31 dB/mm at n_g ~35, respectively. These increase in α reflect structural disordering of the fabricated devices as mentioned above [38].

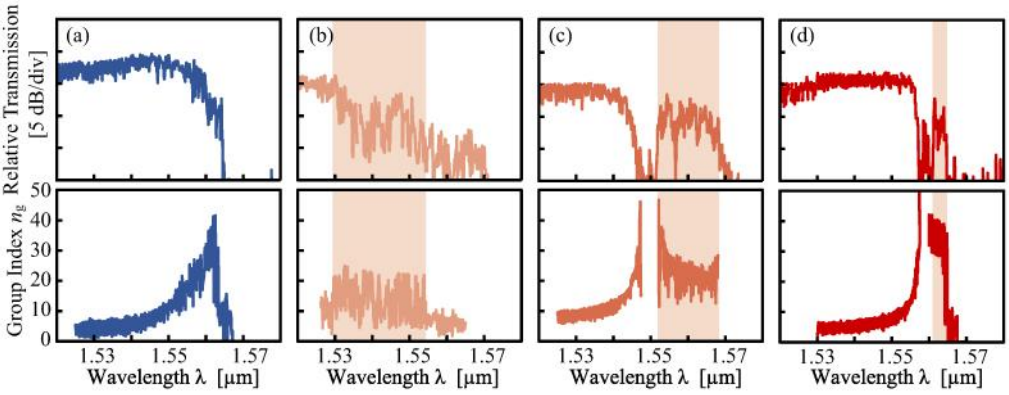

Fig. 4. Transmission and n_g spectra of fabricated ChG PCWs. (a) s/a = 0, $2r/a$ = 0.52, (b) 0.33, 0.53, (c) 0.43, 0.53 and (d) 0.47, 0.53. Light red color indicates LD slow-light band.

C. Pulse transmission

The dispersion of slow light is evaluated through the pulse transmission measurement. Here, sub-ps pulses from mode-locked fiber laser with a 40 MHz repetition are amplified and spectrally expanded using SPM in erbium-doped fiber amplifier (EDFA). They are filtered by tunable band-pass filter at desired center wavelength λ_p (1.53 and 1.56 μm in the high and low v_g regimes, respectively) with desired FWHM bandwidth $\Delta\lambda_p$ (2.0 nm corresponding to a FWHM pulse width τ_p = 2.48 ps), and coupled to the same LS-PCW sample as for Fig. 4(b). The coupling loss from fiber to the waveguide is roughly 20 dB including lens loss. The pulse peak power before coupling, P_{fiber}, and coupled power to the waveguide, P_{in}, are set below 10

#134309 - $15.00 USD Received 31 Aug 2010; revised 22 Sep 2010; accepted 23 Sep 2010; published 6 Dec 2010

W and 0.10 W, respectively, so that we can neglect the SPM in the fiber after the filter and in the sample. The output pulse is observed using autocorrelator. As shown in Fig. 5, τ_p in the high and low v_g regimes are almost the same as the input one. The dispersion constant is no higher than 0.04 fs/nm/mm. Thus, we confirmed that the dispersion is negligible in the devices.

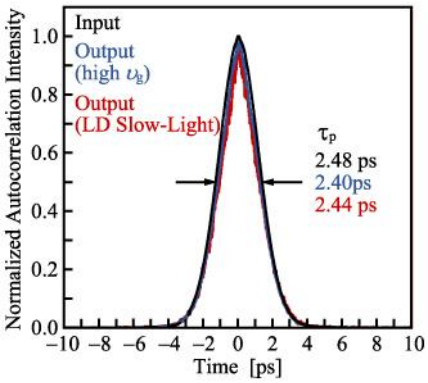

Fig. 5. Autocorrelation traces of input and output pulses for ChG LS-PCW.

5. Nonlinear characteristics

In the nonlinear measurements, the same pulse laser and LS-PCW sample as for Fig. 5 are used.

A. Two-photon absorption

To evaluate TPA, sub-ps pulses from the laser are amplified by EDFA, appropriately attenuated, and coupled to the LS-PCW. To avoid the SPM in the EDFA and fibers, P_{fiber} is set below 200 W, corresponding to $P_{in} < 2$ W. Figure 6 compares the input/output response between the high and low v_g regimes. Neglecting the data fluctuation, almost linear response is observed for both of them. In Si LS-PCWs having the same modal cross-section and length, the saturation of output power appears at $P_{in} > 0.3$ W in the low v_g regime with n_g ~30 [25]. On the other hand, TPA is negligible in this ChG PCW. We also observe that, at $P_{in} > 2$ W, the input facet is damaged such that the line defect nearby the facet is chipped off. Since Ag-As_2Se_3 is transparent and the TPA is negligible at λ ~1.55 μm, we can consider multi-photon absorption, absorption of higher order harmonics and photo-induced mechanical stress as reasons.

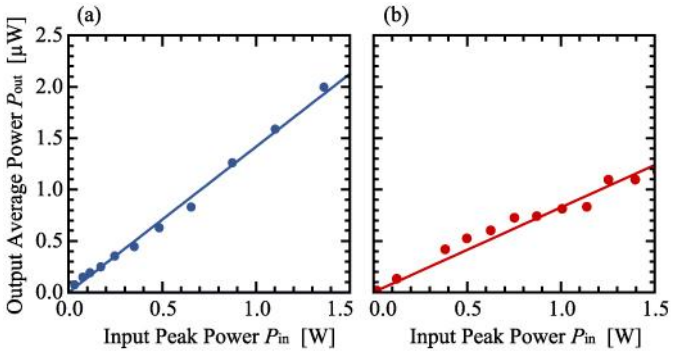

Fig. 6. Input/output response in ChG LS-PCW for evaluating TPA. (a) High v_g regime with n_g ~5 at λ_p = 1.55 μm. (b) LD slow-light regime with n_g ~20 at λ_p = 1.56 μm.

#134309 - $15.00 USD Received 31 Aug 2010; revised 22 Sep 2010; accepted 23 Sep 2010; published 6 Dec 2010

B. Self-phase modulation

The SPM in PCWs is characterized from the spectral change using the same setup as for Fig. 5 and optical spectral analyzer. Figure 7 shows the pulse spectra at different λ_p in a normal PCW (different sample from that for Fig. 4(a)). At $\lambda_p < 1.544$ μm, different spectral shapes at the lowest $P_{in} = 0.5$ W is mainly caused by irregular pulse spectrum generated by the SPM in the EDFA and/or oscillating transmission spectrum of the PCW. When λ_p is close to the band-edge, however, pedestal of the spectrum becomes evident, and the spectral shape changes rapidly with P_{in}. It indicates that the SPM is enhanced by band-edge slow light. Besides, the asymmetric n_g spectrum of the normal PCW might generate asymmetric spectrum of SPM.

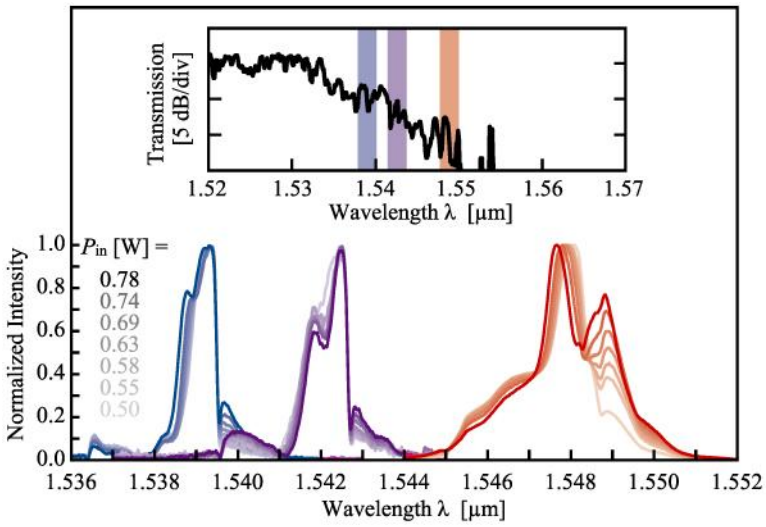

Fig. 7. Change of pulse spectrum caused by SPM near the photonic band-edge in normal ChG PCW.

Figure 8 compares the spectral change between the high and low v_g regimes in the LS-PCW. In the high v_g regime, the spectral peak begins to split into two at $P_{in} > 0.4$ W, and 1.5π nonlinear phase-shift shown by the center dip occurs at $P_{in} = 0.89$ W. In the low v_g regime, on the other hand, the center dip is already observed at $P_{in} = 0.42$ W, and additional peaks appear at higher P_{in}, suggesting a larger phase shift of the SPM enhanced by LD slow light. Different from asymmetric spectral broadening in Fig. 7, Fig. 8 exhibits the relatively symmetric ones. It might reflect the flat n_g spectrum of LS-PCW. It is also different from the case of Si LS-PCWs, i.e. the spectrum particularly broadens toward the short wavelength side due to carrier-plasma effect [42]. The symmetric spectrum in the ChG LS-PCW indicates the pure third-order nonlinearity without carrier effects induced by TPA.

Let us verify the result more quantitatively. In this experiment, P_{in} required for 1.5π phase change is reduced to half when n_g is increased from 10 to 20. The nonlinear phase shift $\Delta\phi_{NL}$ is expressed as

$$\Delta\varphi_{NL} = \frac{{n_g}^2}{A_{eff}} L_{eff} \frac{2\pi n_2}{\lambda_p} P_{in} \qquad (1)$$

where A_{eff} and L_{eff} are the effective modal area and the effective length at $1/e$ power decay, respectively. In Eq. (1), ${n_g}^2$, A_{eff} and L_{eff} can be altered by exploiting LS-PCW. In the experiment, ${n_g}^2$ increased from 10^2 to 20^2, corresponding to 4-fold enhancement. According to the cross-sectional mode analysis, A_{eff} also increases from 0.17 to 0.26 μm^2, leading 0.65-fold reduction. Also, L_{eff} decreases from 0.23 mm (α = 14 dB/mm) to 0.17 mm (α = 21

#134309 - $15.00 USD Received 31 Aug 2010; revised 22 Sep 2010; accepted 23 Sep 2010; published 6 Dec 2010

dB/mm), indicating 0.74-fold reduction. In total, 1.9-fold reduction of P_{in} is estimated, which is in good agreement with the experimental result.

We also estimated the nonlinear parameter $\gamma_{eff} = \Delta\phi_{NL}/P_{in}L_{eff}$, to be 2.3×10^4 and 6.3×10^4 $W^{-1}m^{-1}$ in the high and low v_g regimes, respectively, indicating 2.7-fold enhancement due to LD slow-light. We can confirm the consistency of this value with that expected from structural parameters. Substituting Eq. (1) into above, γ_{eff} is expressed as $\gamma_{eff} = (n_g^2/A_{eff})(2\pi n_2/\lambda_p)$. If the same enhancement and reduction as mentioned above are assumed, 2.6-fold enhancement is evaluated in γ_{eff}. To the best of our knowledge, this γ_{eff} is 200 times larger than 307 $W^{-1}m^{-1}$ for Si wire waveguide [43] and is the largest value for any types of nonlinear waveguides. This is the clear evidence that the ChG slow-light PCWs can be a promising platform for on-chip nonlinear devices.

Furthermore, n_2 of Ag-As_2Se_3 is deduced from γ_{eff} to be as high as ~8×10^{-17} m^2/W. Although n_2 has not been reported for $\lambda = 1.55$ μm, we can reconfirm the result at $\lambda = 1.05$ μm that the Ag doping magnify n_2 of As_2Se_3 to three fold higher [37]. For As_2Se_3, $n_2 = 2.3 \times 10^{-17}$ m^2/W has been measured at $\lambda = 1.55$ μm [15]. According to the above effect of the Ag doping, 6.9×10^{-17} m^2/W is expected for Ag-As_2Se_3, which agrees roughly with the above experimental result.

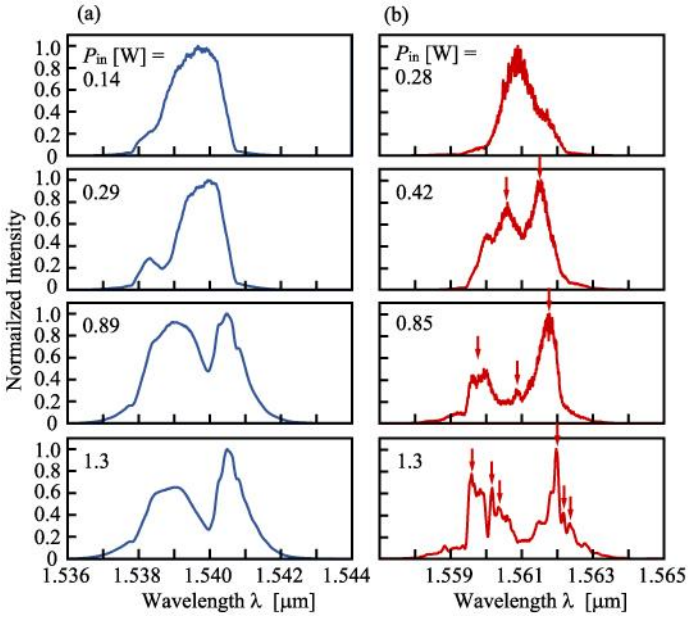

Fig. 8. Spectral change through SPM in ChG LS-PCW in (a) high v_g regime (n_g ~10) and (b) low v_g regime (n_g ~20).

C. Four-wave mixing

To observe the FWM for synchronized two pulses, an optical pulse after the first EDFA is divided into two, each of which are filtered at different λ_p. The timing of the two pulses are adjusted by optical delay line in either arm so that the autocorrelation trace of two pulses after multiplexing shows a clear beat pattern. The multiplexed pulses are launched into the device with P_{in} below the SPM level, and the output spectrum is observed using optical spectrum analyzer. The spectra in two different regimes are shown in Fig. 9. Two idlers are generated from the original signal and pump light. Conversion efficiencies from the signal to the long-wavelength-side idler are –22, –14 and –17 dB in the high and low v_g (n_g ~15, 20) regimes, respectively, i.e. 8 dB improvement by the slow-light effect. Thus it is suggested in this experiment that wide bandwidth LD slow-light waveguide is more advantageous because we

#134309 - $15.00 USD Received 31 Aug 2010; revised 22 Sep 2010; accepted 23 Sep 2010; published 6 Dec 2010

can selectively use minimum dispersion spectrum suitable for phase and group velocity matching.

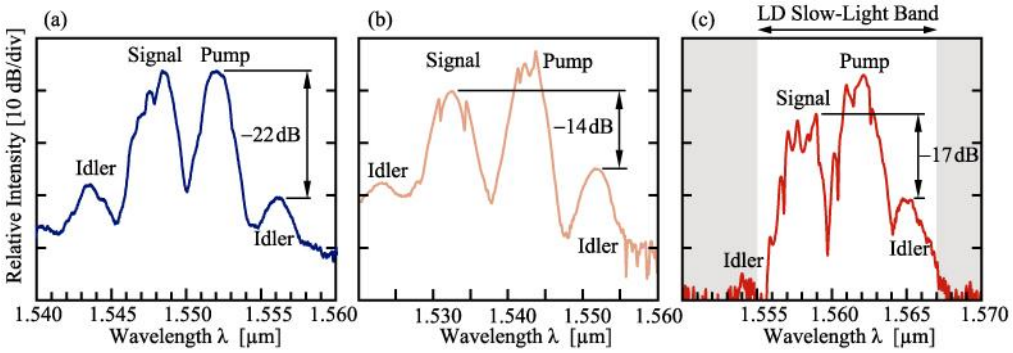

Fig. 9. Observation of FWM in ChG LS-PCW in the (a) high v_g regime (n_g ~5), (b) low v_g regime (n_g ~15) and (c) low v_g regime (n_g ~20).

6. Conclusion

We reported the design, fabrication process and characterization of Ag-As_2Se_3 chalcogenide photonic crystal waveguides. To demonstrate the nonlinearity enhancement due to low-dispersion slow light, we designed and fabricated the third-row lattice-shifted waveguides, and the slow light was confirmed from their group-index spectra and picosecond pulse transmission. We confirmed that two-photon absorption is negligible even with the slow-light enhancement. As for the self-phase modulation, symmetric spectral broadening and central dip were observed, suggesting a 1.5π phase shift. The input power required for this was reduced to half with the slow-light enhancement, which agrees well with theoretical estimates. It suggests a huge effective nonlinear parameter of 6.3×10^4 $W^{-1}m^{-1}$, which is, to our knowledge, the highest value for any nonlinear waveguides. The four-wave mixing was also demonstrated with a conversion efficiency improved from –22 to –14dB due to the slow-light effect. This result is plotted as a red circle in Fig. 1. This study has achieved the optical nonlinearity on highly balanced condition between lower operating power and shorter device length than any other materials and waveguides. Although there are still much room for improving the optical coupling and spectral flatness, these results clearly show its promising potential for high-efficiency and compact on-chip nonlinear devices with ultrafast response.

Acknowledgements

This work was supported from the JSPS Research Fellow-ships for Young Scientists.

#134309 - $15.00 USD Received 31 Aug 2010; revised 22 Sep 2010; accepted 23 Sep 2010; published 6 Dec 2010